Catal Lett (2015) 145:1491–1499
DOI 10.1007/s10562-015-1560-1

SCR of Nitric Oxide by Hydrogen over Pd and Ir Based Catalysts with Different Supports

Chengyang Yin[1] · Lifeng Wang[1] · Sandrine Rivillon[2] · Arthur J. Shih[1] · Ralph T. Yang[1]

Received: 11 March 2015 / Accepted: 3 June 2015 / Published online: 9 June 2015

Abstract Selective catalytic reduction of NO_x with hydrogen (H_2-SCR) in excess oxygen over Pd and Ir based catalysts with various silica supports was studied. The Pd/V_2O_5/TiO_2/SBA-15 and Ir/SBA-15 catalysts showed the highest activities. The effects of noble metal, various silica supports, CO and SO_2 on H_2-SCR over these catalysts were also studied and compared, and possible underlying mechanisms discussed. A comparison of 1 % Ir-doped on silicas with a wide range of pore sizes showed that the peak temperature (where the NO conversion maximum was located) was directly related to the pore size: larger pores of the support resulted in higher peak temperatures. This result indicates that pore diffusion limitation played a role in determining the peak temperature. In addition, a non-noble metal catalyst, Nb_2O_5/SiO_2, was found to have considerable activity.

Graphical Abstract Larger pores of the support resulted in higher peak temperatures, which indicated that pore diffusion limitation played a direct role.

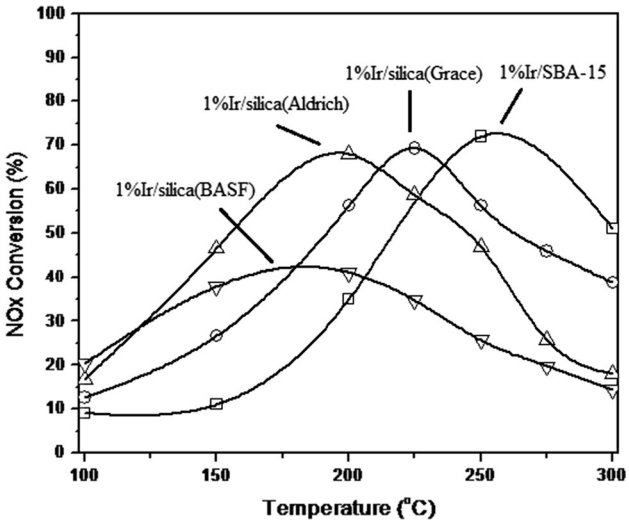

Keywords H_2-SCR · NO_x reduction · Noble metal based catalysts · Silica supports · Carbon monoxide effect on H_2-SCR

1 Introduction

Nitric oxides (NO_x) are major sources of atmospheric pollutants, which are emitted from combustion of fossil fuels in power and chemical processing plants and mobile sources. Removal of NO_x from combustion gases is still a significant challenge which has been extensively studied in the last four decades. The selective catalytic reduction (SCR) of NO_x is one of the most effective methods. The commercial removal of NO_x in power plants is SCR using ammonia as the reducing agent [1–15]. However, some problems remain in the application of NH_3-SCR

✉ Ralph T. Yang
yang@umich.edu

[1] Department of Chemical Engineering, University of Michigan, Ann Arbor, MI 48109, USA

[2] Air Products and Chemicals, Inc., 7201 Hamilton Blvd., Allentown, PA 18195, USA

technology, such as ammonia slip, SO_2 oxidation (by vanadia catalysts), and air heater and equipment fouling by the formation of a "white powder" (i.e., ammonium compounds such as bisulfate, sulfate and nitrate….) as well as SO_3.

Recently, SCR of NO_x by H_2 (H_2-SCR) has attracted attention for NO_x removal [16–35]. In H_2-SCR, hydrogen is used as the reducing agent, by which NO_x can be reduced effectively at lower temperatures ($T < 300$ °C) as compared with ammonia-SCR which operates at near 350 °C. The products of H_2-SCR are without other hazardous gas formation which makes it more environmentally friendly.

Hydrogen is present in (engine) exhaust and it is formed mainly by the water–gas shift reaction with CO. Indeed, H_2-SCR is one of the reactions taking place in the three-way converters (TWC) over noble metal catalysts [36]. Also present in the exhaust gas is CO which may also participate in the SCR of NO, or, CO-SCR. Thus, the effects (or role) of CO in H_2-SCR have been of interest, and it has been shown that the presence of CO has a significant influence on H_2-SCR [23, 31–35]. The presence of CO has a significant promoting influence for some catalysts (e.g., Pd and Ir) while negative effects for others (such as Pt).

In this work, catalysts with Pd, Ir and Nb_2O_5 doped on different supports were tested for their catalytic activities for H_2-SCR. More specifically, they were tested for NO reduction in combustion gases from the combustion of methane (or natural gas). Thus, a simulated methane combustion gas containing 50 ppm NO was used in all tests. The effects of CO on H_2-SCR were also studied. The effects of noble metal, different supports, CO and SO_2 on the catalytic activities over these catalysts were investigated for possible practical applications. More specifically, this was a catalyst screening study for applications in the temperature window of 200–250 °C.

2 Experimental

Mesoporous silicas with various pore sizes and pore volumes were used as the support. A large-pore silica, SBA-15, was synthesized, while three commercial silica gels with a wide range of pore sizes were included: 28 Å (from BASF), 67 Å (from Aldrich) and 154 Å (from Grace, designated as Grade 59 silica). The SBA-15 was synthesized by following the procedure in the literature [37]. Briefly, Pluronic P123 was used as the template and was dissolved in water and HCl solution while stirring at room temperature, then 1, 3, 5-trimethylbenzene was added. Then tetraethyl orthosilicate (TEOS) was added into above solution. After being aged overnight, the resultant precipitates were filtered, washed, dried and calcined. The Barrett–Joyner–Halenda (BJH) average pore size of the resulting SBA-15 was 200 Å.

2.1 Catalysts Preparation

2.1.1 1 %Pd/Silica Catalyst

1 %Pd/silica(Grace) was prepared via incipient wetness impregnation of silica from Grace in an aqueous solution of tetraamminepalladium(II) chloride monohydrate ($Pd(NH_3)_4Cl_2 \cdot H_2O$, 99.99 + %, Aldrich). The impregnated sample was dried at 60 °C for 24 h to evaporate part of the water, then transferred to an oven at 100 °C and heated for 24 h. Finally, it was calcined in air at 500 °C for 6 h [38].

2.1.2 $Pd/V_2O_5/TiO_2/SBA$-15

First, the 20 %TiO_2/SBA-15 (all percentages are wt%) was prepared by hydrolysis of a solution of titanium(IV) n-butoxide ($Ti[O(CH_2)_3CH_3]_4$, 98 + %, Strem Chemicals) in the presence of SBA-15. Then the 5 %V_2O_5/20 %TiO_2/SBA-15 was prepared by impregnation of the above TiO_2/SBA-15 with a solution of ammonium metavanadate (NH_4VO_3, 99 %, Sigma-Aldrich) in oxalic acid. Finally, 1 % palladium was impregnated on 5 %V_2O_5/20 %TiO_2/SBA-15 using a $Pd(NH_3)_4Cl_2$ solution. The catalyst was then dried at 120 °C overnight and calcined in air at 500 °C for 6 h.

2.1.3 Ir/Silica Catalyst

The mixture of iridium(III) chloride hydrate ($IrCl_3 \cdot xH_2O$, Aldrich) aqueous solution and a silica gel (from Grace, Aldrich or BASF) was stirred for 24 h. The mixture was then transferred to an oven at 60 °C and heated for 24 h to evaporate most of the moisture, and then transferred to an oven and heated at 100 °C for 24 h. Finally, the sample was calcined at 600 °C in air flow for 8 h [39].

2.1.4 Nb_2O_5/Silica and 1 % Ru/Nb_2O_5/Silica Catalysts

The 10 %Nb_2O_5/silica(Grace) was prepared via incipient wetness impregnation of silica from Grace with an aqueous solution of ammonium niobate(V) oxalate hydrate ($C_4H_4NNb_bO_9 \cdot xH_2O$, 99.99 %, Aldrich). The impregnated sample was dried at 60 °C for 24 h, then transferred to an oven and heated at 100 °C for 24 h, and finally calcined in air at 400 °C for 6 h. Subsequently 1 % ruthenium was impregnated on 10 %Nb_2O_5/silica(Grace) using a ruthenium(III) nitrosyl nitrate ($RuNO(NO_3)_3$, Aldrich) solution. The catalyst was dried at 100 °C overnight and calcined at 400 °C for 6 h in air. A bimetallic Ir-Ru catalyst with 0.5 % iridium and 0.5 % ruthenium was also prepared by

impregnating on 10 %Nb_2O_5/silica(Grace) using $IrCl_3$ solution and ruthenium nitrosyl nitrate solution. The catalyst was also dried at 100 °C overnight and calcined in air at 400 °C for 6 h. Calcination temperature of 400 °C for Nb_2O_5 was due to obtain strong Brønsted acidity of Nb_2O_5. However, higher temperature will destroy the acidity of Nb_2O_5 [40].

2.2 Characterization and Catalytic Activity Tests

Micromeritics ASAP 2020 sorptometer was used to measure the N_2 adsorption isotherms of the samples at liquid N_2 temperature (−196 °C). The specific surface area was determined from the linear portion of the BET plot. Prior to the surface area and pore size distribution measurements, the samples were degassed in vacuo at 350 °C for 12 h. The surface areas were calculated by using the Brunauer–Emmett–Teller (BET) method based on the adsorption data. The pore size distribution or the average pore size was calculated by using the BJH method.

Transmission electron microscopy (TEM) images of the samples were obtained on a JEOL 3011 electron microscope which was operated at 300 kV.

The catalytic activity measurement was carried out in a fixed-bed quartz reactor. The reactant gas was a simulated flue gas from natural gas combustion with the following composition: 50 ppm NO, 1.5 % O_2, 17.5 % H_2O, and balance He. It also contained 2000 ppm H_2, added as the reductant. 200 mg of sample was used in each run. The total flow rate was either 100 or 200 mL/min (measured under ambient conditions). The NO and NO_2 concentrations were continually monitored by a NO/NO_x analyzer (Thermo Environmental Instruments, Inc.). At each reaction temperature, the NO_x conversion and product analysis were measured after 1–2 h (for reaching a steady state) depending on the reaction. The product N_2 selectivity was analyzed by using a Shimadzu gas chromatograph with a 13X molecular sieve column (for N_2) and a Porapak Q column (for N_2O).

3 Results and Discussion

3.1 NO_x Reduction over Different Catalysts

The performance of all the catalysts for NO_x reduction with H_2 in the presence of excess oxygen (1.5 % O_2) were tested. Although 17.5 % H_2O was also added, it has been shown that its addition led to only very slight decreases in the SCR activities during 5-hour runs for a number of catalysts [33]. The peak activities (i.e., peak activities on the conversion vs. temperature profiles) of these catalysts are shown in Table 1. The NO_x conversion of these catalysts increased with temperature and reached their peak activities around 200–250 °C, subsequently NO conversion decreased with temperature when the temperature was further increased to 300 °C. (The phenomenon of having two temperature peaks for Pd was first observed and explained by Ueda et al. [17]). The NO_x conversion over Pd/V_2O_5/TiO_2/SBA-15 was 95 % at 200 °C and the N_2 selectivity over Pd/V_2O_5/TiO_2/SBA-15 was 85 %.

For Pd based catalysts exposed to temperatures higher than the maximum peak temperature (e.g., at 250 °C), the NO conversion decreased by two mechanisms [17]. (1) The consumption of H_2 by excess O_2 became dominant, which caused NO_x conversion to begin to decrease. (2) The second mechanism is related to thermodynamics. It is well established that NO_2 is considerably more active than NO in the ammonia-SCR reaction, as shown, for example, by Long and Yang [41]. The reaction $NO + 1/2O_2 = NO_2$ favors lower temperature and becomes the limiting step at higher temperatures because less NO_2 is formed [41]. It has also been shown that, like the ammonia-SCR reaction, the H_2-SCR reaction is also limited by the thermodynamic equilibrium of NO oxidation at higher temperatures. Details of the peaking phenomenon has been studied by Ueda et al. [17].

The kinetics of the H_2-SCR reaction on a similar Pd-supported catalyst, Pd/V_2O_5/TiO_2/Al_2O_3, was studied with a differential reactor by Qi et al. [24]. Under excess O_2 (2 %), the rate of NO conversion was 0.92th-order with respect to NO concentration, i.e., approximately first-order. Thus, the SCR activity can be represented quantitatively by the apparent first-order rate constant (k). By assuming plug flow reactor (in a fixed bed of catalyst) and free of diffusion limitation, the apparent rate constant can be calculated from the NO conversion (X) by

$$k = -\frac{F_0}{[NO]_0 W} \cdot \ln(1 - X), \quad (1)$$

where F_0 is the molar NO feed rate, $[NO]_0$ is the molar NO concentration in the feed at the reaction temperature and W is the catalyst amount (g). From the NO conversions and reaction conditions, the first-order rate constants could be calculated. For example, the k value for the Pd/V_2O_5/TiO_2/SBA-15 catalyst was 79.25 cm^3/g/s at 200 °C, which is the highest k value of these catalysts and hence the most active.

The Pd/V_2O_5/TiO_2/SBA-15 catalyst was very similar to the Pd/V_2O_5/TiO_2/Al_2O_3 catalyst that we have studied previously [24], with the only difference being in the support (silica vs. Al_2O_3). The activities were also similar. The mechanism was studied by in situ FTIR which showed ammonium ions (NH_4^+, formed on the Brønsted acid sites of V_2O_5) as the key intermediate that underwent fast reactions with NO/O_2 to form N_2 [24]. Apparently the

Table 1 Catalytic performance of various catalysts

Catalyst	Peak T (°C)	NO conv. (%)	First-order rate constant (k)[a] ($cm^3/g/s$)
1 %Pd/silica(Grace)	150	63	11.76
$Pd/V_2O_5/TiO_2$/SBA-15[b]	200	95	79.25
1 %Ir/SBA-15	250	72	37.23
1 %Ir/silica(Grace)	225	69	16.31
1 %Ir/silica(Aldrich)	200	68	15.07
1 %Ir/silica (BASF)	200	41	6.98
10 %Nb_2O_5/silica(Grace)	250	56	11.88
1 %Ru/Nb_2O_5/silica(Grace)	225	60	12.76
0.5 %Ir–0.5 %Ru/Nb_2O_5/silica(Grace)	225	63	13.85

[a] Reaction conditions: 200 mg catalyst. 50 ppm NO, 2000 ppm H_2, 1.5 % O_2, 17.5 % H_2O and balance He. The total flow rate was 100 mL/min

[a] First-order rate constant, defined by Eq. (1)

[b] The flow rate was 200 mL/min

same mechanism operated for the $Pd/V_2O_5/TiO_2$/SBA-15 catalyst.

The N_2 product selectivity refers to the fraction of the NO conversion that leads to N_2 formation, while the other reaction product is N_2O. The $Pd/V_2O_5/TiO_2$/SBA-15 catalyst also showed high N_2 selectivity values (80–85 %) in the temperature range of 150–250 °C, which is a wide temperature window of operation in the presence of excess oxygen (1.5 % O_2). The N_2 selectivity was 85 % at 200 °C when the maximum NO_x conversion of 95 % was reached. The high N_2 selectivity was possibly related to the acidic property of the V_2O_5/TiO_2/SBA-15 supports. The compatible acidic supports may provide a higher N_2 selectivity for the H_2-SCR [21]. Further discussion on N_2 selectivity will follow.

3.2 Comparisons of Different Noble Metals and Different Supports

Figure 1 shows the conversions of NO_x over the 1 %Ir/silica(Grace) and 1 %Pd/silica(Grace) catalysts. Both samples showed some activity. As discussed in the literature, Pd showed two temperature peaks while Ir showed a single temperature peak [27, 42]. Silica was used for this comparison because it was shown to yield the highest H_2-SCR activity for Ir supported catalysts on various supports (TiO_2, Al_2O_3, ZSM-5 and silica) [27].

At 225 °C, the maximum NO conversion over 1 %Ir/silica(Grace) was 70 % and the conversion over 1 % Pd/silica(Grace) was ~50 %. However, at the lower temperatures, the Pd-doped catalyst showed higher activities than Ir doped catalyst [27], e.g., 63 % at 150 °C.

For Ir doped catalysts, Hamada and coworkers established that SiO_2 was the best support compared with other supports (Al_2O_3, TiO_2 and H-ZSM-5) [27, 43]. A commercial silica gel with BET surface area 300 m^2/g was used as the support in their work. In this work, we compared 1 % Ir/SiO_2 using four silica samples with a wide range of pore sizes and surface areas. The results showed different activities and more interestingly, different NO conversion—temperature profiles. After calcination, the four silica samples are still very stable [37].

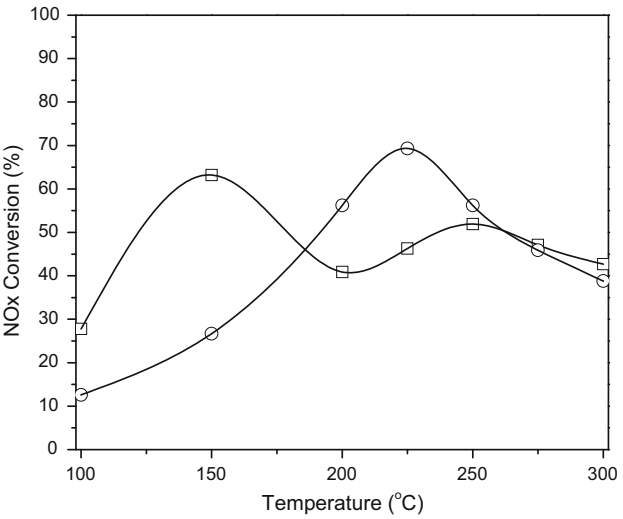

Fig. 1 NO_x conversions over 1 %Pd/silica(Grace) (*open square*) and 1 %Ir/silica(Grace) (*open circle*). Reaction conditions: 50 ppm NO, 2000 ppm H_2, 1.5 % O_2, 17.5 % H_2O and balance helium, 200 mg catalyst, flow rate 100 mL/min

The BET surface areas, pore sizes and pore volumes of the four silicas are listed in Table 2. The BET surface areas of the metal doped catalysts were nearly the same as that of the supports, apparently due to the small amounts of doped metals (i.e., 1 wt%). The NO conversions at various temperatures are shown in Fig. 2. Both peak temperature and the NO conversion at the peak temperature are different for

Table 2 Textural parameters of various supports

Support	BET surface area (m^2/g)[a]	Pore size (Å)[b]	Pore volume (cm^3/g)[c]
SBA-15	560	200	1.58
Silica (Grace)	280	154	1.11
Silica (Aldrich)	361	67	0.78
Silica (BASF)	743	28	0.25

[a] Calculated from the linear part of the BET plot

[b] BJH adsorption average pore width

[c] BJH adsorption cumulative volume of pores

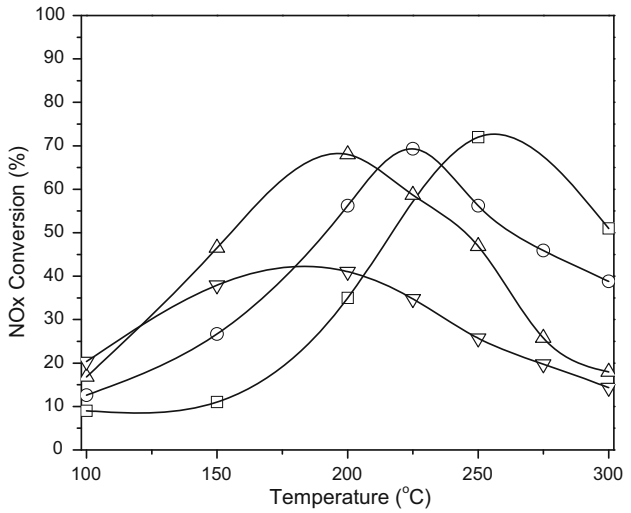

Fig. 2 NO_x conversions over 1 %Ir/SBA-15 (*open square*), 1 %Ir/silica(Grace) (*open circle*), 1 %Ir/silica(Aldrich) (*open triangle up*) and 1 %Ir/silica(BASF) (*open triangle down*). Reaction conditions: 50 ppm NO, 2000 ppm H_2, 1.5 % O_2, 17.5 % H_2O and balance helium, 200 mg catalyst, flow rate 100 mL/min

these four Ir-doped samples. The peak temperature is shifted towards a higher temperature as the pore size was larger, i.e., Ir/SBA-15 with the largest pore size (20 nm) showed the highest peak temperature, while it decreased as the pore size was smaller. This result may be interpreted based on two aspects: metal dispersion and pore diffusion limitation.

XRD analysis of the four Ir-doped samples showed no peak at $2\theta = 41°$, i.e. Ir(111) diffraction (as seen by Haneda et al. for 1 % Ir/SiO2 on low-dispersion samples with dispersion <46 % [44]). Clearly the Ir nanoparticle sizes were limited by the sizes of the pores of the silica support in which Ir was impregnated (i.e., the pore sizes of all three commercial silica gels were less than 15.4 nm, as shown in Table 2). The SBA-15 silica had the largest pore size, 20 nm and had possibly the largest Ir particle sizes. TEM images showed that the Ir nanoparticles supported on SBA-15 had sizes of approximately 15–20 nm (Fig. 3a). The Ir sizes were limited by the sizes of the pores of the other 3 silica gels: 15.4 nm for Grace SiO_2, 6.7 nm for Aldrich SiO_2 and 2.8 nm for BASF SiO_2. TEM images also showed that the Ir nanoparticles supported on different silica support had different Ir sizes. The Ir nanoparticles supported on Grace SiO_2 had sizes of approximately 15 nm (Fig. 3b), supported on Aldrich SiO_2 had sizes of approximately 6 nm (Fig. 3c) and supported on BASF SiO_2 had sizes of approximately 2.5 nm (Fig. 3d). The BJH pore size decreased slightly upon doping of 1 wt% Ir. On the silica gel with the smallest pores, the BASF silica, the BET surface area, average pore size and pore volume were, respectively, 743 m^2/g, 28 Å, and 0.25 cm^3/g. After doping 1 % Ir, these values were 589 m^2/g, 27 Å and 0.19 cm^3/g. Thus, the slight decreases in these values confirmed that doping 1 wt% Ir resulted in only slight pore plugging even for the silica with the smallest pore sizes.

The temperature dependence of the overall rates of the catalyzed reactions taking place inside porous structures has been well understood [45]. In the low temperature range, the overall rate is limited by the surface reaction inside the pores, and the temperature dependence follows the Arrhenius law. At higher temperatures, the pore diffusion rate becomes involved and the rate-controlling step: this is because pore diffusion has a weaker (and different) temperature dependence [45, 46] than that of the Arrhenius Law, hence the overall rate enters the pore-diffusion-control regime.

As discussed above, two reasons (H_2 combustion and thermodynamic limit for NO_2 formation) contribute to the decline in the NO conversion beyond the peak temperature. Our result on the dependence of the peak temperature on the pore size indicates a third contributing step: pore diffusion limitation. This result indicates that the onset temperature for the pore-diffusion-limitation regime also played a role in determining the peak temperature for NO conversion. The silica support with the smallest pore sizes (BASF, 2.8 nm before doping, or 2.7 nm after 1 %Ir doping), in which diffusion (of the molecules of the reactants and products) was the slowest compared with the other silica samples, entered the pore-diffusion-limitation regime at the lowest temperature, and showed the lowest peak temperature for NO conversion. For the other silica samples with larger pores, pore diffusion was faster, so the

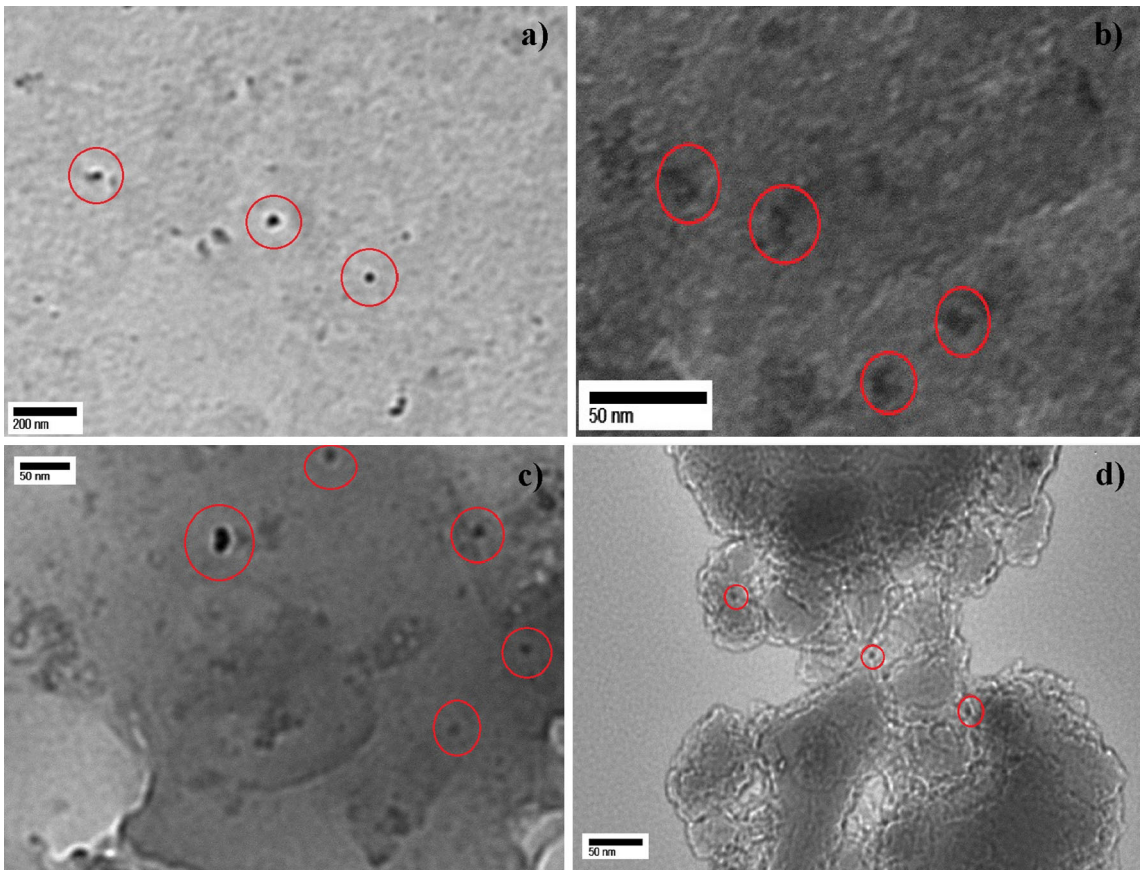

Fig. 3 TEM images of iridium supported on different silica support, **a** 1 %Ir/SBA-15, **b** 1 %Ir/silica(Grace), **c** 1 %Ir/silica(Aldrich) and **d** 1 %Ir/silica(BASF). *Scale bar* 200 nm for **a**, 50 nm for **b**–**d**

onset temperature for entering the pore-diffusion-control regime was higher. The other two factors, as mentioned, caused the decline in NO conversion beyond the peak temperature. For more in-depth discussions on the interplay of reaction–diffusion in catalyzed reactions taking place in porous catalysts, please see, for example, Refs. [45, 46].

At temperatures below the peak temperature, i.e., in the kinetic-control regime, metal dispersion contributed to the differences in NO conversion. At 100 °C, the NO conversion was inversely related to the pore size: BASF silica (2.8 nm pore size) showed the highest NO conversion, followed by Aldrich silica (6.7 nm) > Grace silica (15.4 nm) > SBA-15 (20 nm). This result indicates that higher metal dispersion contributed towards higher NO conversion.

As mentioned above, the N_2 product selectivity has been studied. N_2 selectivity depends on the metal, temperature, support and gas composition (e.g., the presence of SO_2, CO….). Between the most studied metals (i.e., Pt and Pd), the N_2 selectivities on Pd are generally higher than that on Pt. On supported Pt, the N_2 selectivities were generally below 60 % [17, 27] while that on supported Pd were above 80 % [24, 27, 33]. However, 0.1 % Pt/MgO–CeO_2 showed ~90 % N_2 selectivity and it depended on H_2/NO ratio in the reactant gas [47]. In our work, the N_2 selectivity on 0.3 %Ir–2 %Ru/silica(Grace) was 79.3 % at 225 °C, which was typical for supported Ir catalysts [27].

3.3 Nb_2O_5

Nb_2O_5 has been reported to be an effective promoter for NH_3-SCR of NO because of its strong Brønsted acidity as well as redox capability [13, 48, 49]. The Nb_2O_5 doped on silica(Grace) was tested for its activity for H_2-SCR, without any noble metal. Likewise, it was also tested for its activity as a promoter for Ir and Ru.

Figure 4 shows the conversion of NO_x over the following catalysts: 10 %Nb_2O_5/silica, 1 %Ru/Nb_2O_5/silica and 0.5 %Ir–0.5 %Ru/Nb_2O_5/silica (all three SiO_2 were from Grace). It is interesting to note that the doped Nb_2O_5 had considerable activity, particularly at 250–300 °C. We have previously shown Zn-ZSM-5 as a non-noble metal catalyst for H_2-SCR. Nb_2O_5 is yet another non-noble metal catalyst. At lower temperatures, the doped Ir and Ru both

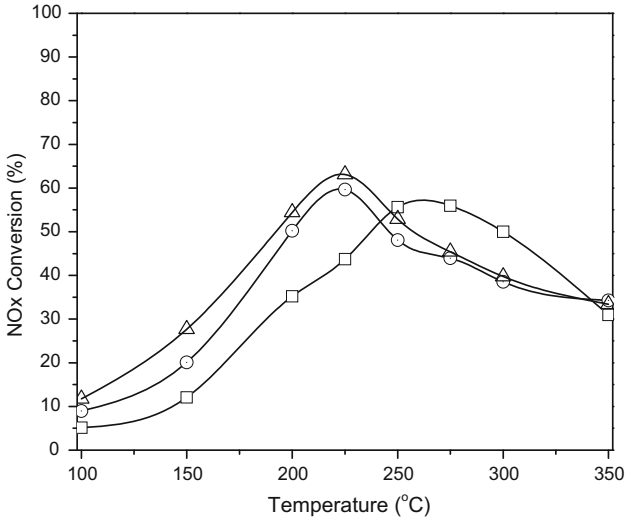

Fig. 4 NO_x conversions over 10 %Nb_2O_5/silica(Grace) (*open square*), 1 %Ru/Nb_2O_5/silica(Grace) (*open circle*), and 0.5 %Ir–0.5 %Ru/Nb_2O_5/silica(Grace) (*open triangle up*). Reaction conditions: 50 ppm NO, 2000 ppm H_2, 1.5 % O_2, 17.5 % H_2O and balance helium, 200 mg catalyst, flow rate 100 mL/min

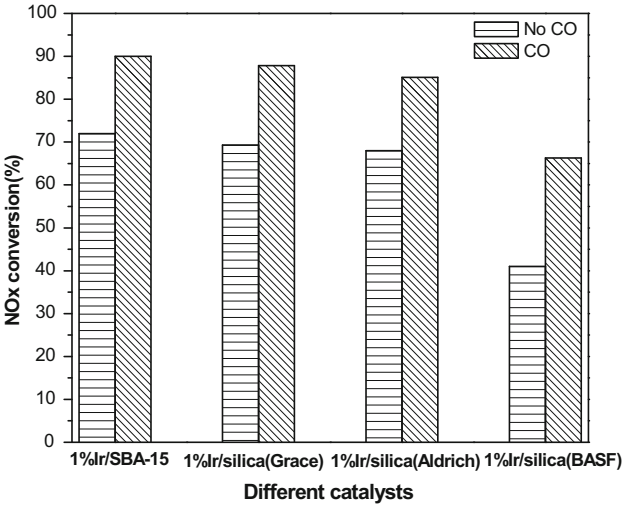

Fig. 5 CO effect on NO_x conversion over 1 %Ir/SBA–15, 1 %Ir/silica(Grace), 1 %Ir/silica(Aldrich) and 1 %Ir/silica(BASF). Reaction conditions: 50 ppm NO, 2000 ppm H_2, 1.5 % O_2, 17.5 % H_2O, 1000 ppm CO (when used) and balance helium, 200 mg catalyst, flow rate 100 mL/min

showed higher activities than Nb_2O_5/silica. The conversion over 0.5 %Ir–0.5 %Ru/Nb_2O_5/silica(Grace) was 63 % at 225 °C, and that over 10 % Nb_2O_5/silica(Grace) was 56 % at 250 °C. The mechanism for H_2-SCR on the Nb_2O_5/silica catalyst is subject of further study.

3.4 Effects of CO

Selective catalytic reduction of NO_x in excess O_2 using CO as the reductant (i.e., CO-SCR) has also been studied. In fact, CO-SCR takes place in the three-way catalytic converter [36]. For H_2-SCR, the effect of CO is a complex one, depending on the noble metal. CO could have a strong poisoning effect (e.g., on Pt) while it could have a significant promoting effect (e.g., on Pd). The promoting effects of CO on Pd-doped catalysts, in particular, have been studied by several groups [23, 34, 35]. Macleod and Lambert [34] attributed the effect by the formation of HNCO intermediate which was formed on Pd in a mixture of H_2/CO/NO [50].

To study the effect of CO on H_2-SCR over the Ir/SiO_2 catalysts, CO with 1000 ppm was added to the reactant gas. The SCR reaction temperature was set to the respective peak temperature. As shown in Fig. 5, the NO_x conversion increased in the presence of CO over these 1 %Ir/SiO_2 catalysts. The NO_x conversion-temperature profiles for the 1 %Ir/SiO_2 (SBA-15) are shown in Fig. 6. The enhancements in NO_x conversion by CO were seen at all temperatures.

Interestingly, enhancement in NO conversion for H_2-SCR by added CO was observed only for Pd/Al_2O_3, not for

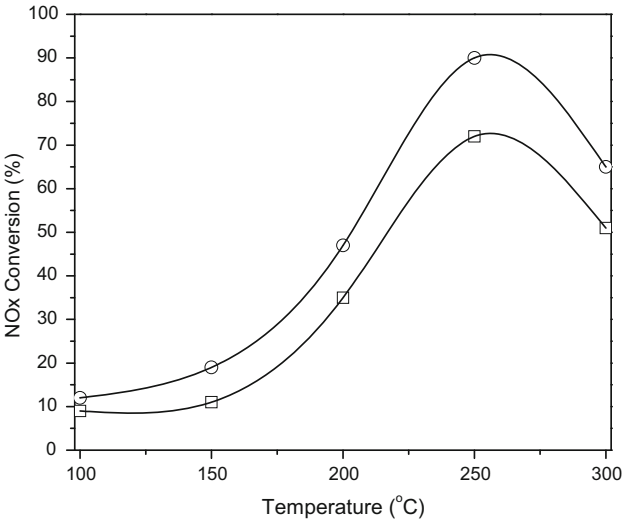

Fig. 6 NO_x conversions over 1 %Ir/SBA-15, no CO (*open square*) and with 1000 ppm CO (*open circle*), Reaction conditions: 50 ppm NO, 2000 ppm H_2, 1.5 % O_2, 17.5 % H_2O and balance helium, 200 mg catalyst, flow rate 100 mL/min

Pd/SiO_2 [34]. The intermediate HNCO undergoes hydrolysis (to form NH_3) only on Al_2O_3 (as observed by Dumplemann et al. [51]). Upon formation of NH_3, the SCR reaction switched to the NH_3-SCR route, which is faster than H_2-SCR. Thus, our results cannot be explained by the formation of HNCO.

The extensive studies of Hamada et al. [27] on CO-SCR showed that Ir and Rh doped catalysts were the most active, and that, again, the SiO_2 supported Ir and Rh yielded the highest conversion. Thus, the results shown in

Figs. 5 and 6 could be attributed to combined H_2-SCR and CO-SCR. Possible interplays between these two reactions merit further investigation.

3.5 Effects of SO_2

Effect of SO_2 is of practical importance, thus it is studied for selected catalysts. The effects of SO_2 on NO_x conversion over 1 %Ir/SBA-15 at 250 and 300 °C are shown in Fig. 7. The positive effect of SO_2 was also observed for H_2-SCR over Ir/SiO_2 catalyst by Hamada et al. [27]. Our earlier work also showed enhancements of the NH_3-SCR activity by SO_2 on V_2O_5/TiO_2 catalyst [52]. Based on molecular orbital calculation results, the enhancement was attributed to the increased Brønsted acidity on the V_2O_5 surface by the adsorption of SO_2 [52]. The enhancement in the H_2-SCR activity by the adsorbed SO_2 on Ir/SiO_2 could possibly be attributed to the increased Brønsted acidity.

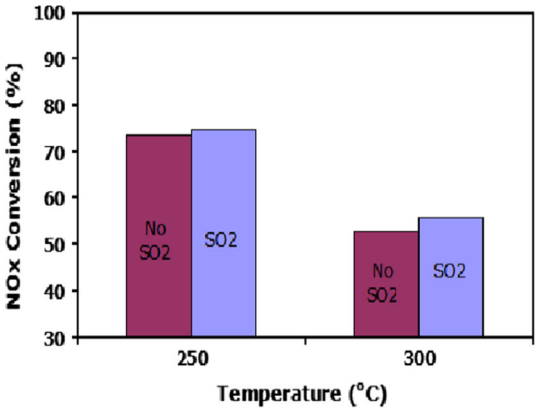

Fig. 7 SO_2 effect on NO_x conversion over 1 %Ir/SBA-15 at 250 and 300 °C. Reaction conditions: 50 ppm NO, 2000 ppm H_2, 1.5 % O_2, 10 ppm SO_2, 17.5 % H_2O and balance helium, 200 mg catalyst, flow rate 100 mL/min

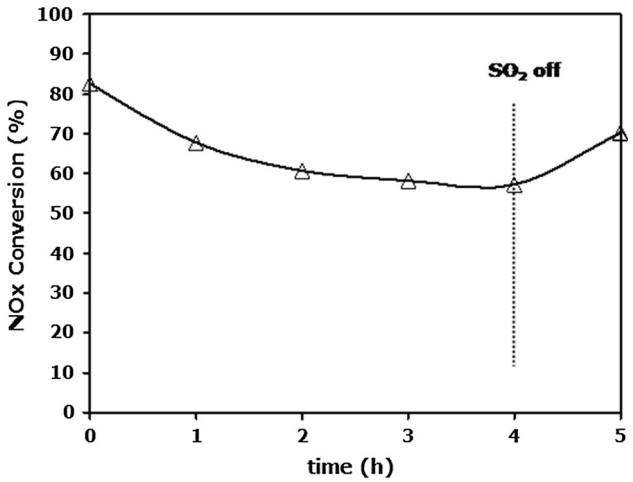

Fig. 8 SO_2 effect on NO_x conversion over $Pd/V_2O_5/TiO_2/SBA-15$. Reaction conditions: 50 ppm NO, 2000 ppm H_2, 1.5 % O_2, 1000 ppm CO, 17.5 % H_2O, 7.5 ppm SO_2, balance helium, 200 mg catalyst, flow rate 200 mL/min

However, a deactivation effect of SO_2 was observed for H_2-SCR for the $Pd/V_2O_5/TiO_2/SBA-15$ catalyst, as shown in Fig. 8. At 250 °C, when SO_2 was added to the reactant gas, the NO_x conversion over $Pd/V_2O_5/TiO_2/SBA-15$ decreased steadily from 82 to 56 % in 4 h. The deactivation was reversible as also shown in Fig. 8.

4 Conclusions

Selective catalytic reduction of nitric oxide with H_2 in the presence of excess oxygen was studied over Ir or Pd doped catalysts using various silica supports. A simulated flue gas from combustion of methane was used as the reactant gas. The $Pd/V_2O_5/TiO_2/SBA-15$ and Ir/SBA-15 catalysts showed the highest H_2-SCR activities. Pd doped silica showed higher activity than Ir doped silica at low temperatures (<170 °C) while Ir showed higher activities at higher temperatures (>200 °C). A non-noble metal catalyst, Nb_2O_5/SiO_2, was found to have considerable activity. A comparison of 1 % Ir-doped on silicas with a wide range of pore sizes showed that the peak temperature (where the NO conversion maximum was located) was directly related to the pore size: larger pores of the support resulted in higher peak temperatures. This result indicates that pore diffusion limitation played a direct role in determining the peak temperature. The addition of CO in the reactant gas showed a strong enhancement in the NO conversion for all Ir doped catalysts, a clear indication that CO-SCR also took place. The addition of SO_2 increased the activities for the Ir-doped catalyst while had a deactivation effect on the Pd-doped catalyst.

Acknowledgments The authors thank Air Products and Chemicals for funding of this project.

References

1. Cai Y, Ozkan US (1991) Appl Catal 78:241–255
2. Kumthekar MW, Ozkan US (1997) Appl Catal A 151:289–303
3. Choi EY, Nam I-S, Kim YG (1996) J Catal 161:597–604
4. Kim YJ, Kwon HJ, Heo I, Nam I-S, Cho BK, Choung JW, Cha M-S, Yeo GK (2012) Appl Catal B 126:9–21
5. Wang J, Yu T, Wang X, Qi G, Xue J, Shen M, Li W (2012) Appl Catal B 127:137–147
6. Xue J, Wang X, Qi G, Wang J, Shen M, Li W (2013) J Catal 297:56–64
7. Fritz A, Pitchon V (1997) Appl Catal B 13:1–25
8. Busca G, Lietti L, Ramis G, Berti F (1998) Appl Catal B 18:1–36
9. Lobree LJ, Hwang I-C, Reimer JA, Bell AT (1999) J Catal 186:242–253
10. Long RQ, Yang RT (1999) J Am Chem Soc 121:5595–5596

11. Long RQ, Yang RT (2001) J Catal 198:20–28
12. Qi G, Gatt JE, Yang RT (2004) J Catal 226:120–128
13. Qu R, Gao X, Cen K, Li JH (2013) Appl Catal B 142–143:290–297
14. Brandenberger S, Krocher O, Tissler A, Althoff R (2008) Catal Rev 50:492–531
15. Granger P, Parvulescu VI (2011) Chem Rev 111:3155–3207
16. Hecker WC, Bell AT (1985) J Catal 92:247–259
17. Ueda A, Takayuki N, Masashi A, Kobayashi T (1998) Catal Today 45:135–138
18. Burch R, Coleman MD (1999) Appl Catal B 23:115–121
19. Costa CN, Savva PG, Andronikou C, Lambrou PS, Polychronopoulou K, Belessi VC, Stathopoulos VN, Pomonis PJ, Efstathiou AM (2002) J Catal 209:456–471
20. Burch R, Coleman MD (2002) J Catal 208:435–447
21. Shibata J, Hashimoto M, Shimizu K, Yoshida H, Hattori T, Satsuma A (2004) J Phys Chem B 108:18327–18335
22. Machida M, Watanabe T (2004) Appl Catal B 52:281–286
23. Qi G, Yang RT, Thompson LT (2004) Appl Catal A 259:261–267
24. Qi G, Yang RT, Rinaldi FC (2006) J Catal 237:381–392
25. Costa CN, Efstathiou AM (2007) Appl Catal B 72:240–252
26. Wu P, Li L, Yu Q, Wu G, Guan N (2010) Catal Today 158:228–234
27. Hamada H, Haneda M (2012) Appl Catal A 421–422:1–13
28. Yokota K, Fukui M, Tanaka T (1997) Appl Surf Sci 121–122:273–277
29. Rodríguez GCM, Saruhan B (2010) Appl Catal B 93:304–313
30. Costa CN, Savva PG, Fierro JLG, Efstathiou AM (2007) Appl Catal B 75:147–156
31. Savva PG, Costa CN (2011) Catal Rev Sci Eng 53:91–151
32. Liu Z, Li J, Woo SI (2012) Energy Environ Sci 5:8799–8814
33. Wang L, Chen H, Yuan M-H, Rivillon S, Klingenberg EH, Li J, Yang RT (2014) Appl Catal B 152–153:162–171
34. Macleod N, Lambert RM (2002) Appl Catal B 35:269–279
35. Haneda M, Chiba K, Takahashi A, Sasaki M, Fujitani T, Hamada H (2007) Catal Lett 118:159–164
36. Taylor KC (1984) Automobile catalytic converters. Springer, Berlin, pp 13–16
37. Zhao D, Huo Q, Feng J, Chmelka BF, Stucky GD (1998) J Am Chem Soc 120(24):6024–6036
38. Sato S, Takahashi R, Sodesawa T, Koubata M (2005) Appl Catal A 284:247–251
39. Tamai T, Haneda M, Fujitani T, Hamada H (2007) Catal Commun 8:885–888
40. Tanabe K, Misono M, Ono Y, Hattori H (1989) New solid acids and bases. Elsevier, Amsterdam
41. Long RQ, Yang RT (2000) J Catal 194:80–90
42. Li J, Wu GJ, Guan NJ, Li LD (2012) Catal Commun 24:38–44
43. Yoshinari T, Sato K, Haneda M, Kintaichi Y, Hamada H (2001) Catal Commun 2:155–158
44. Haneda M, Fujitani T, Hamada H (2006) J Mol Catal A 256:143–148
45. Fogler HS (2005) Elements of chemical reaction engineering. Prentice Hall, Englewood Cliff **Ch12**
46. Satterfield CN (1980) Heterogeneous catalysis in practice. McGraw-Hill, New York **Ch11**
47. Olympiou GG, Efstathiou AM (2011) Chem Eng J 170:424–432
48. Vikulov KA, Andreini A, Poels EK, Bliek A (1994) Catal Lett 25:49–54
49. Lian Z, Liu F, He H, Shi X, Mo J, Wu Z (2014) Chem Eng J 250:390–398
50. Voorhoeve RJH, Trimble LE (1978) J Catal 54:269–280
51. Dumplemann R, Cant NW, Trimm DL (1996) J Catal 162:96–103
52. Chen JP, Yang RT (1990) J Catal 125:411–420